Biogeochemistry of U, Ni, and As in two meromictic pit lakes at the Cluff Lake uranium mine, northern Saskatchewan

Konstantin von Gunten[1], Tyler Warchola[1], Mark W. Donner[2], Manuel Cossio[1], Weiduo Hao[1], Christopher Boothman[3], Jonathan Lloyd[3], Tariq Siddique[2], Camille A. Partin[4], Shannon L. Flynn[1], Arden Rosaasen[5], Kurt O. Konhauser[1], Daniel S. Alessi[1]

[1]Department of Earth and Atmospheric Sciences, University of Alberta, 1-26 Earth Sciences Building, Edmonton, T6G 2R3, Canada

[2]Department of Renewable Resources, University of Alberta, 751 General Services Building, Edmonton, Alberta, T6G 2H1, Canada

[3]School of Earth and Environmental Sciences, University of Manchester, Oxford Road, Manchester, M13 9PL, United Kingdom

[4]Department of Geological Sciences, University of Saskatchewan, 114 Science Place, Saskatoon, Saskatchewan, S7N 5E2, Canada

[5]AREVA Resources Canada, 817 45 St W, Saskatoon, Saskatchewan, S7K 3X5, Canada

1 Abstract

Open pits, which remain after uranium (U) mining operations cease, can form meromictic lakes which develop suitable conditions for the containment of dissolved and colloidal metals. In this study, the distribution and speciation of U, nickel (Ni), and arsenic (As) in the water column of two meromictic pit lakes was investigated at the decommissioned Cluff Lake mine in northern Saskatchewan. The 28 m deep and older D-pit had a chemocline at 13 m depth, below which it turned anoxic and its meromixis was controlled by iron (Fe) cycling. Below the chemocline both Fe(III) and As(V) were reduced to Fe(II) and As(III), respectively. Iron cycling had a large effect on U distribution because reducing conditions prevented sulfide oxidation and a drop in pH in deeper layers. Metal-reducing bacteria were found to be present at, and below, the chemocline. In the deeper (90 m), larger and more recently flooded DJX-pit, two chemoclines were observed at depths of 15 and 65 m. Both were linked to sharp U and Ni concentration gradients. Unlike the D-pit, a transition to reducing conditions was not observed in the DJX-pit's water column. However, colloidal U, primarily associated with aluminum

oxyhydroxides, was found below the first chemocline. Overall, the meromixis-type determined the distribution and speciation of metals and bacteria in the investigated pit lakes, thus providing insights into the use of pit lakes as a potential bioremediation strategy.

Les cavités subsistantes après l'extraction d'uranium (U) forment souvent des lacs méromictiques contaminés avec des métaux. La distribution et la spéciation de U, nickel (Ni) et arsenic (As) a été étudiée dans deux lacs méromictiques à Cluff Lake, une mine au nord du Saskatchewan. Le lac D-pit (28 m) était plus âgé et possédait une chimiocline à 13 m, sous laquelle il devenait anaérobique, cette stratification étant contrôlée par le fer (Fe), qui, ainsi que le As changeait de spéciation sous cette limite. Le cycle du Fe influençait la distribution de U et les conditions réduites sous la chimiocline prévenaient d'une chute du pH. Des bactéries réductrices de métaux ont été trouvées au niveau et sous la chimiocline. Dans le plus grand lac, DJX-pit (90 m), se trouvait deux chimioclines (15 m et 65 m). Les deux étaient concomitantes à de forts gradients de concentrations de U et de Ni. Contrairement au D-pit, aucune transition redox n'a été observée, mais des colloïdes transportant de l'uranium principalement lié avec des oxyhydroxides d'aluminium ont pu être mis en évidence sous la première chimiocline. La méromicticité et les conditions d'oxydo-réductions contrôlaient donc la distribution et la spéciation des métaux et métalloïdes, ainsi que des bactéries. Ils offrent de nouveaux aperçus de l'utilisation des lacs méromictics pour la bioremédiation.

Keywords: meromixis, pit lakes, uranium mining, redox, colloidal metal transport

2 Introduction

2.1 Objectives

Canada is one of the largest uranium (U) producers in the world. The U mining process exposes excavated rock to surface oxidizing conditions, which can result in the mobilization and accumulation of metals and metalloids in nearby environments. Knowledge of the geochemical processes and reactions of potential contaminants at former mine sites is important to mitigate impacts from future

mining operations. Despite the significant literature pertaining to U transport and bioremediation in laboratory studies and temperate field environments, such as the Rifle site in Colorado (Williams *et al.*, 2011; Bargar *et al.*, 2013; Alessi *et al.*, 2014) and the Oak Ridge site in Tennessee (Watson *et al.*, 2013; Leigh *et al.*, 2014), little is known about the transport and fate of U in subarctic regions, such as those where Canada's U resources are mined. Arsenic (As) and nickel (Ni) are often found to be associated with U deposits and can become major contaminants in mining districts (Donahue *et al.*, 2000). Accordingly, our motivation was to study U, Ni, and As mobility and speciation in two chemically-stratified (meromictic) pit lakes in a subarctic climate at the decommissioned Cluff Lake mine, located in the Athabasca Basin in northern Saskatchewan (Figure 1). These lakes are two examples of mine pit lakes with different histories, sizes, geometries, stratification behaviors and U, Ni, and As metal distributions. Additionally, this study investigates the role of colloidal particles in the geochemical cycling of those metals.

2.2 Geological setting

Cluff Lake is located in Canada's most important uranium mining region, the Paleo- and Mesoproterozoic Athabasca Basin, which contains the highest-grade U deposits in the world (Donahue *et al.*, 2000) (Figure 1). The Athabasca Basin deposits are hosted in either crystalline basement rocks or within the overlying sandstone of the Athabasca Group (Kyser and Cuney, 2008). The basement orthogneisses at the Cluff Lake site were exposed during the formation of the Carswell structure in the Paleozoic (Harper, 1981). The U is predominantly found as uraninite-sulfide (dated at ~1150 Ma), uraninite-Te-Se-Bi (~1050 Ma), pitchblende-sulfide, and pitchblende-hematite (both ~380 Ma) (Bell, 1985; Ruhlmann, 1985). The ore found in the Athabasca Basin contains high grades of Ni (up to 2%) and As (up to 1.2%) due to the presence of primary minerals gersdorffite, niccolite, bravoite, and chalcopyrite (Donahue *et al.*, 2000).

2.3 Characteristics of the pit lakes: D-pit and DJX-pit

In this study, we focused on two pit lakes at the Cluff Lake site (Figure 1): D-pit (formed 34 years ago) and DJX-pit (formed 15 years ago). Mining of D-pit occurred between 1979 and 1981 (AREVA, 2009), during which time the nearby Boulder Creek was diverted to allow for pit development. In 1983 the creek overflowed during spring thaw and flooded the D-pit (AREVA, 2009). A waste rock pile located adjacent to the pit was revegetated between 1983 and 1985, but minor metal leaching from the covered waste pile has been reported (AREVA, 2009). The D-pit lake has a surface area of 15,400 m^2 and an approximate depth of 28 m.

The DJX-pit was composed of two open pits: DJN-Pit, which was mined from 1989 to 1991, and DJX-pit, mined from 1994 to 1997. To develop the DJN-Pit, the adjacent Claude Creek was diverted into the nearby Peter River. The DJN-Pit was subsequently used for waste rock disposal (containing <0.03% U) from the adjacent DJX-pit, which showed high potential for acid generation (AREVA, 2009). After mining ceased in the DJX-pit, it was seasonally dewatered to minimize water inflow to the nearby DJ underground mine (1994-2002). With the cessation of mining, the DJN-pit and the DJX-pit were flooded with water from the adjacent Cluff Lake (AREVA, 2009), and today they form one water body, which will hereafter be referred to as DJX-pit. The water level in the 90 m deep pit has stabilized below the level of nearby Cluff Lake, forming a pit lake with a surface area of approximately 85,900 m^2 (AREVA, 2013).

Additional information on hydrology and climate, as well as the extent of the Cluff Lake mine areas and on historical sampling records can be found in Section 1 of the supplementary information (SI). Relevant information on U biogeochemistry can be found in Section 2 of the SI.

2.4 Importance of colloids and meromixis

When metal speciation in natural environments is studied, it is important to consider that metals are often associated with colloidal particles between 1 nm and 1 μm in size (Dai *et al.*, 1995). Colloids can

play an important role at abandoned mining sites, as the revegetation of such areas can increase the abundance of low molecular weight acids which can interact with Fe-, Al- and Si-bearing phases in soils and enhance colloid formation (Slowey *et al.*, 2007). Such colloids can consist of organic carbon or oxyhydroxide aggregates containing Fe, Al, Si, or P, and crucially, they can increase the transport of metals under conditions that typically inhibit mobility (Dai *et al.*, 1995; Kretzschmar and Schäfer, 2005; Wang *et al.*, 2013).

In general, when U ore is extracted from open pit mines, the mine pits can eventually fill with surface runoff (e.g., spring melt), rain- and groundwater, forming pit lakes. A characteristic feature of these pit lakes are the steeply sided walls and considerable depth (Schultze *et al.*, 2016). Relative depth is often calculated for pit lakes, which is defined as the ratio of the maximum depth to the circular diameter of the surface (Pieters and Lawrence, 2014). Such lakes can become meromictic, whereby the water body is separated by a chemocline into an upper mixolimnion that expresses seasonal turnover, and a lower monimolimnion with limited water exchange with the overlaying water mass. These layers vary considerably in density and chemical composition. The formation of meromixis depends on various factors, in addition to the shape of the lake basin, including protection against wind, climatic conditions, ice melt and runoff, and groundwater inputs (Pieters and Lawrence, 2014; Schultze *et al.*, 2016; Boehrer *et al.*, 2017). Meromixis is not always a stable condition; the regular mixing of the mixolimnion can push the chemocline down, whereas the turnover of the monimolimnion, initiated by the input of less saline groundwater or geothermal heating, can lead to its rise (Pieters and Lawrence, 2014). The selective manipulation of the meromixis stability can be used as a pit lake remediation tool, and has been applied for the containment of highly contaminated brines and acid mine drainage (Geller *et al.*, 2012). Nevertheless, published meromixis related geochemical data are scarce and not all geochemical relations are well understood (Schultze *et al.*, 2016).

3 Materials and Methods

3.1 Water sampling and measurement of field parameters

In June 2016, water was sampled from D-pit and DJX-pit from a boat in the center of the pit. A plastic tube was lowered into the pit together with a measuring tape and the probe of a multi-parameter water quality meter (YSI Professional Plus). D-pit was sampled from 0.5-23 m in 1 m intervals, while DJX-pit was sampled from 0.5-82 m in 2 to 5 m intervals. Temperature, pH, oxidation-reduction potential (ORP), dissolved oxygen, and conductivity were recorded using the water quality meter at each depth. Sampled water was pumped through the tubing using a MasterFlex E/S portable sampler (Cole-Parmer) and collected in the boat.

For metal quantification and arsenic speciation analysis, the water was filtered (0.45 µm nylon membranes, Agilent Technologies) and collected into acidified (0.05 M HCl) 50 mL polypropylene (PP) tubes (Fisher Scientific), which were wrapped in aluminum foil to prevent photo-oxidation of redox-sensitive species. For carbon, nitrogen, and anion analyses, unfiltered water samples were collected without acidification. Separate non-acidified samples, filtered through 0.45 µm membranes, were collected into 250 mL polypropylene copolymer (PPCO) centrifuge bottles (Thermo Fisher), wrapped in aluminum foil, for asymmetrical flow field-flow fractionation (AF4). For iron speciation, 1 mL of water was directly filtered (0.45 µm) into 2 mL Eppendorf tubes and acidified with 1 mL of 2 M HCl for preservation. Results, collected in June 2016, were compared to preliminary field measurements (temperature, pH, conductivity) and water analyses (selected depths for cations, anions, carbon, and nitrogen, only) conducted in September of 2015 using similar methods (exception: 0.2 µm filters used). Field measurements for DJX-pit were also performed in September 2016. Groundwater was sampled in June 2016 from wells located close to the two investigated pits (Figure S1). The well south of D-pit was DWW0041G (7 m deep, N 58.3617°, W 109.5154°) and will hereafter be referred to as groundwater well 1 (GW1). Two groundwater wells close to the DJX-pit were sampled: the well

147 north of the DJX-pit (GW2) is labeled as MNW6210G (17 m deep, N 58.3709°, W 109.5494°) and the
148 well west of the DJX-pit (GW3) is labeled as HYD9846AG (4 m deep, N 58.3675°, W 109.5489°).
149 Three well volumes were pumped to adequately purge the well before sampling (Vail, 2013).

150 ### *3.2 Water chemistry*

151 The unfiltered and unacidified water samples were analyzed for total carbon (TC), total inorganic
152 carbon (TIC), and total nitrogen (TN) using a Shimadzu TOCV-N CHS/SCN Model Total Organic
153 Carbon Analyzer with potassium nitrate and potassium hydrogen phthalate as calibration standards,
154 and potassium acid phthalate certified reference material for quality control (detection limit: 0.1 ppm).
155 Total organic carbon (TOC) was calculated by determining the difference between TC and TIC. Splits
156 of the same samples were filtered (0.45 μm) for anion analysis by ion chromatography using a DX 600
157 (Dionex) with a 4 mm analytical column AS9-HC and a guard column AG9-HC (detection limit: 0.2-
158 1.0 ppm). Filtered and acidified water samples were analyzed with an Inductively Coupled Plasma
159 Mass Spectrometer (ICP-MS/MS) Triple Quadrupole system (Agilent Technologies 8800). Single-
160 element standards (Spex CertiPrep, Ricca Chemical Company) were diluted in 2% HNO_3 (trace metal
161 grade, Fisher Scientific) and 0.5% HCl (trace metal grade, Fisher Scientific), and used for external
162 calibration. See Table S2 (SI) for all used analyte masses and MS/MS modes.

163 ### *3.3 Speciation of metals and metalloids*

164 Selected samples (filtered, preserved in 1 M HCl) from both pits were subjected to a standard ferrozine
165 assay based on the methods of Stookey (1970), Viollier *et al.* (2000), and Porsch and Kappler (2011),
166 in order to determine iron speciation. Total Fe-content was determined by adding 400 μL of
167 hydroxylamine hydrochloride (10% in 1M HCl) to 100 μL of each sample (preserved in 1 M HCl),
168 which were left for 30 min in the dark. 500 μL of ferrozine (0.1% in 50% ammonium acetate) were
169 added, followed by another 5 min incubation in the dark. Fe(II) concentrations were determined by
170 adding 400 μL of 1M HCl to 100 μL of each sample, followed by 500 μL of ferrozine. After 5 min of

incubation time in the dark, the samples were analyzed on the spectrophotometer. The ferrozine complex was quantified spectrophotometrically at 562 nm using an Evolution 60S UV-Vis Spectrophotometer (Thermo Scientific). Calibration curves for total Fe and Fe(II) (0 to 1000 µM) were generated using $(NH_4)_2Fe(SO_4)_2 \cdot 6H_2O$ in 1M HCl, and confirmed by ICP-MS/MS.

Filtered and acidified samples were analyzed using a high performance ion chromatograph (IC; Thermo Scientific Dionex ICS-5000$^+$) paired with a quadrupole inductively coupled plasma mass spectrometer (iCAP Q ICP-MS, Thermo Scientific) operated in kinetic energy discrimination mode with helium as the collision gas. Arsenic species were separated using a Dionex Ion Pac AS7 anion exchange column (4 mm ID x 250 mm length) and AG7 guard column (4 mm ID x 50 mm length), with dilute HNO_3 as the mobile phase. Samples were also analyzed for total concentrations of trace metals using an iCAP Q ICP-MS. More detailed method information can be found in Donner *et al.* (2017). Thermodynamic modeling of metal speciation was conducted using the PHREEQC 3.3.7 software and the Minteq (2009) database. Modeling was done for D-pit at depths of 0.5 m, 5 m, 10 m, 13 m, and 20 m, and for DJX-pit at 0.5 m, 50 m, and 80 m. For the inputs, measured cation and anion concentrations (in mol/L), pH, and oxidation-reduction potential (ORP) values were used (see Table S11 for more details).

3.4 Asymmetrical flow field-flow fractionation

Filtered water samples collected for colloidal analysis were analyzed for the distribution of metals in the dissolved and colloidal (oxyhydroxides and organic matter) fractions. The analysis was completed using asymmetrical flow field-flow fractionation (AF4) equipped with an auto injector (AF200 and PN5300, respectively, Postnova Analytics), coupled to a UV-Visible absorbance detector (G4212 DAD, Agilent Technologies) and a quadrupole inductively-coupled mass spectrometer (iCAP Q ICP-MS; Thermo Scientific). The AF4 fractionation procedure is described elsewhere (Guéguen and Cuss, 2011). Ultrapure water and HCl were used to adjust the pH and conductivity of the ultrapure

ammonium carbonate carrier fluid buffer (Sigma-Aldrich) in order to match the properties of the analyzed samples. Specifically, these adjustments were pH 7 and a conductivity of 300 µS/cm for D-pit and DJX-pit surface samples, and pH 6 and 1500 µS/cm for DJX-pit deep water samples based on Neubauer *et al.* (2013). The areas of the free, organic matter-associated, and oxyhydroxide-associated peaks were determined using statistical deconvolution as described in Cuss and Guéguen (2012).

3.5 16S-rRNA gene profiling

Prokaryotic diversity in the pit lakes was determined using 16S rRNA gene sequencing on selected unfiltered water samples from September 2015. DNA was extracted from the water samples using the PowerWater DNA Isolation Kit (Mobio). Fifteen mL of each water sample was filtered through 0.2 µm membranes using a vacuum unit and the membranes were processed according to kit instructions. Sequencing was performed by a dual-index paired-end sequencing approach on an Illumina MiSeq sequencer based on the method by Kozich *et al.* (2013). Post processing was done using a pipeline consisting of the following applications: Cutadapt and FastQC (quality control), Sickle (quality trimming), SPADes (Illumina MiSeq errors correction), Pandaseq (merging of paired reads), Qiime with UPARSE and Vsearch (removal of singletons and chimeras, building of OTU tables and phylogenetic trees, and for Shannon diversity).

4 Results

4.1 Limnology of D-pit and DJX-pit

Schematic diagrams of D-pit and DJX-pit can be seen in Figure 2, and are useful for understanding the different scales of the two locations. In September 2015, D-pit expressed one thermocline around 5 m and one major halocline between 12-13 m, accompanied by a pH decrease from 8.1 to 7.8 (Figure 3, left column). In June 2016, D-pit expressed a similar halocline at 12-15 m depth. Between 2-12 m depth a pH decrease from pH 7.3 to 6.2 was recorded. The dissolved oxygen concentrations in D-pit increased slightly within the first 2 m, decreased rapidly between 2-5 m, and then continued to

decrease at a less rapid rate between 5-10 m. Corresponding to the oxygen curve, the ORP dropped from +200 mV (oxic conditions) to -300 mV (reducing conditions) between 12-20 m of depth. In this case, the upper 15 m can be referred to as mixolimnion, which by definition is affected by seasonal mixing.

The DJX-pit showed a thermocline between 0-10 m in all data sets (Figure 3, right column). In June 2016, the depth of the thermocline was similar to September 2015, but was associated with a stronger temperature gradient. Across all data sets, four haloclines were identified around the following depths: 5 m, 17 m, 55 m, and 65 m. The halocline at 5 m depth was closely associated with an increase in oxygen (e.g., up to 11.6 mg/L in June 2016), likely due to primary production, which was followed by an oxygen decline to 20 m (as low as 4.4 mg/L) and a more moderate decline to the bottom (<0.9 mg/L). The pH was generally lower than in D-pit and decreased from pH 7.5 at 5 m depth to pH 5.5 below the halocline at 17 m depth. In the DJX-pit, the ORP was positive throughout the measured column (150-280 mV), which may result from redox interactions, e.g., by Mn(III/IV), NO_3^- (Schürling *et al.*, 2013) or even sulfate, because under low pH conditions, sulfate-reducing environments might result in higher measured ORP values (Church *et al.*, 2007, Falagán *et al.*, 2013).

4.2 Distribution of metals and ligands

In the D-pit, total carbon was 22 ppm at the surface, rising to 47 ppm at 17 m (Figure 4, left column and Table S7). It was dominated by inorganic species; organic carbon remained between 4-13 ppm. No phosphate was detected in D-pit, likely due to precipitation with Fe (Jaeger, 1994). Sulfate was detectable above 13 m, coinciding with the depth of the halocline and the change of the ORP from positive to negative. Below this depth, no SO_4^{2-} or NO_3^- could be detected, however, N was present, indicating that more reduced nitrogen species are present. The reduction of SO_4^{2-} can result in the precipitation of iron sulfide phases with low solubility, forming in the presence of Fe^{2+} and the negative ORP below the chemocline (Sobolewski, 1999). In the D-pit, concentrations of B, Na, Mg, K,

Ca, Mn, and Fe increased with depth (Table S5 and Figure 4, left column). A significant increase in Fe concentrations was observed below 12 m depth, coinciding with a drop in ORP values and oxygen concentrations. This suggests that there was a shift towards Fe(III)-reducing conditions, as supported by the Fe speciation results discussed below. Further, Mn concentrations steadily increased from 0.2 ppm to 3.3 ppm. Nickel concentrations were low at the surface of the D-pit, with a concentration maximum of 9 ppb measured at the chemocline; Ni then became undetectable below 15 m (Figure 4, left column). The As concentration profile was similar to that of Fe, with the former increasing in concentration with depth from 2 ppb to 91 ppb and showing a small decrease at 20 m (76 ppb). The concentration profile of U was strongly linked to changes in pH. The drop to pH 6.2 between 4 and 12 m was associated with a decrease in U concentrations from 120 ppb at the surface to 64 ppb at 7 m depth. Below 11 m, U concentrations increased with increasing pH to 131 ppb (13 m) and stabilized below 16 m to around 90 ppb. A similar concentration trend was observed for Si (Table S5).

In the DJX-pit, total carbon ranged from 5.4-13.8 mg/L (Figure 4, right column and Table S8). DJX-pit carbon composition was similarly dominated by inorganic carbon; however, this trend reversed after 70 m, where the presence of organic carbon became more predominant. TOC was generally lower in deeper water layers of the DJX-pit compared to D-pit, in conjunction with the presence of oxygen. Sulfate-S values reached 78 mg/L at the 15 m halocline, up to 172 mg/L in the upper monimolimnion, and up to 476 mg/L near the bottom of the pit (82 m). Trace amounts of Se, V, Cd, Pb, Sb, Tl were detected by iCAP Q ICP-MS (Table S12). The deep water of DJX-pit was rich in B, Na, Mg, K, Ca (dominant metal), and Mn, but depleted in Fe compared to the D-pit (Figure 4, right column and Table S6). This pattern was likely due to the presence of oxygen in the deep-water layers of DJX-pit, leading to the precipitation of Fe(III) oxyhydroxides. Concentration curves of U, Ni, and Mn had similar shapes, with the two major chemoclines evident at 15 m and 65 m (Figure 4, right

column). Based on the high Mn concentrations, the bottom water layers of DJX-pit were potentially in the redox transition zone between oxic and Mn(IV)-reducing conditions.

In general, the DJX-pit metal concentration profiles indicate that stratification is an important control for metal distribution. A slight decrease was observed in the concentrations of U, Ni, and Zn (also Cu, as shown in Table S6), which could indicate the beginning of the development of an anoxic zone below 82 m, where those metals might be precipitating as sulfides. Supporting this conclusion are the trace amounts of As at 80 m depth, which are nearly double those at the surface of the DJX-pit (Table S12). The lower chemocline (65 m) was sharp, and was well developed for most metals in the DJX-pit (exceptions: Li, Al, and Si). This lower zone could be due to remnant mine water from the time when the pit was used for temporary mine water storage prior to being flooded with freshwater from Cluff Lake. Arsenic and Fe concentrations were low (<2 ppb and <28 ppb, respectively) throughout the water column. Results for DJX-pit obtained in September 2015 indicated higher Fe concentrations (4.6 ppm at 70 m, see Table S3) compared to the June 2016 results (7 ppb), while Mn concentrations were marginally lower (3.6 ppm vs. 3.9 ppm at 70 m). Oxygen concentrations in the DJX-pit were lower in September 2015 (personal communication, CanNorth), suggesting that the bottom of the DJX-pit is not consistently oxygenated every year (see section 5.1).

Metal concentrations, anions, carbon, and nitrogen results for the three sampled groundwater wells are shown in Tables S5-S8 (SI). A Piper diagram showing the water composition of these samples in relation to the pit water samples is shown in Figure S6. The well GW1, close to D-pit, was rich in Na (2.2 ppm), Mg (7.2 ppm), and Ca (11.4 ppm), while the Fe concentration was only 0.5 ppm. Well GW2, located at the northern end of DJX-pit, was rich in Na (125.9 ppm), Mg (49.5 ppm), K (12.5 ppm), and Ca (155.4 ppm), and had higher concentrations of Fe and Br compared to the pit water. GW3 had, in general, lower metal concentrations.

The relative abundance of Al, Fe, As, and Ni in the water columns of the two pits match well with the concentrations found in the adjacent rock samples (SI, Section 3 and Table S14). Rock samples and the water in DJX-pit had high concentrations of Al and Ni, while D-pit rock samples and water were more enriched in Fe and As. Some elements, however, showed opposite trends, such as Zn, Mn, and U.

4.3 Speciation of metals

In D-pit, Fe(II) concentrations increased with depth, with 78-80% of total Fe as Fe(II) in deeper water layers (Table 1). The results for D-pit demonstrate that there is a distinct shift in Fe speciation towards Fe(II) species below the depth where the ORP switches from positive to negative near 12 m. The groundwater close to D-pit (GW1) was dominated by Fe(III), with only 31% Fe(II). In DJX-pit, neither Fe(II) nor total Fe were detected by the ferrozine method, and only traces of Fe could be found using ICP-MS/MS. Water in well GW3, located west of the DJX-pit, also had no detectable Fe.

IC-ICP-MS for D-pit samples showed the abundance of As(III) and As(V). In general, the sum of As(III) and As(V) were close to the total As concentration at each depth (Table 2). A marked shift in As speciation was observed between depths of 10 m to 13 m. The high concentrations of As in the D-pit below the chemocline are the result of the reducing conditions in the monimolimnion, which not only promote the reduction of Fe(III) but also the reduction and release of any bound As(V) species to the more mobile As(III) form. Arsenic speciation determination was problematic in the DJX-pit due to the presence of unknown As species and their co-elution with known peaks at determined retention times.

Thermodynamic modeling with PHREEQC showed a charge balance difference of >10% close to the D-pit chemocline and below (Table S11), indicating that not all charge bearing components were fully identified and modeled. For example, colloid-bound metals and organometallic species might have a strong influence due to their abundance and high surface charge. As shown in Table 3, the model predicted the dominant U(VI) species to be $UO_2(CO_3)_2^{2-}$ and $UO_2CO_3^0$ for the top 10 meters of

each pit. In D-pit, at the chemocline and at 20 m depth, $U(OH)_5^-$ was expected to dominate, whereas in the DJX-pit, $UO_2CO_3^0$, UO_2^{2+}, and $UO_2SO_4^0$ were predicted to become the dominant species in deeper layers. In the D-pit, the saturation index was positive for U_4O_9, UO_2, and $USiO_4$ at and below the chemocline. In the DJX-pit, U_3O_8 and U_4O_9 were saturated at 80 m depth. Precipitation of U(IV) species may explain the observed concentration drops in the D-pit of U and Si below 13 m depth (Table S5). Compared to IC-ICP-MS results, As(V) species were overestimated for the D-pit surface water and underestimated for the deeper water layers. On the other hand, As(III) species were underestimated by the calculations above the chemocline at 13 m depth. $HAsO_4^{2-}$ and $H_2AsO_4^-$ were calculated to be the dominant As species in the DJX-pit at all depths. Nickel was predicted to be predominately $NiCO_3^0$ in the D-pit (up to 96%) and Ni^{2+} in the DJX-pit (up to 80%), but in the DJX-pit, due to high SO_4^{2-} concentrations, $NiSO_4^0$ (up to 28%) was also predicted.

4.4 Colloidal metal fractions

Colloidal fraction analyses for D-pit indicated high variability with depth with regards to the distribution of metals between free ions, dissolved organic matter (DOM) and oxyhydroxide fractions (Tables S9 and S10). For most of the metals investigated, the free ion phase was the dominant species. An exception was Al, which was predominantly in the DOM and oxyhydroxides size fractions, which may indicate the presence of colloidal aluminosilicates (Filella, 2006). This was particularly evident in D-pit, where DOM contributed up to 67% (5 m) of the Al, while oxyhydroxide contributions made up the remaining 33% (0.5-5 m). In contrast, in the DJX-pit the DOM size fraction (up to 59%) and the oxyhydroxide fraction (up to 23%) only played a role in Al partitioning in the surface waters (0.5-10 m).

For U, Ni, and As, the colloidal distribution in the two pit lakes was different (Figure 5). In the mixolimnion of the D-pit, U was mostly associated with the oxyhydroxide size fraction (up to 12%), with a small contribution by DOM (up to 3%). At 0.5 m, 5 m, and 10 m, there was a progressive

increase for U in the oxyhydroxide size fraction with 0%, 7%, and 12% being colloidal, respectively (Figure 5). This fraction then dropped to 2% at the chemocline. This pattern was inversely related to the pH (Figure 3) and U concentrations (Figure 4) in the mixolimnion of the D-pit. Nickel was scarce in the D-pit water column, however, up to 34% of Ni in the mixolimnion, and all Ni found at 20 m depth was in colloidal form (DOM). For As in the D-pit, the oxyhydroxide size fraction played an important role, hosting up to 42% of the total As in the oxic water layers. Below the chemocline (13 m) As was mostly found as a free ion, suggesting that in contrast to U, As was not binding to reduced particulate organic matter.

In the DJX-pit, colloidal U (associated with oxyhydroxides) was only relevant in the samples below the upper chemocline (>30 m) where it contributed approximately 16% of total U. The same colloidal material also carried minor amounts of Al (0.9-1.8 ppb), but no Fe or Mn (Table S10), which might indicate that the U-bearing colloids were Al oxyhydroxides. Despite high (>2.1 ppm) Ni concentrations below 20 m depth of the DJX-pit, colloidal Ni was only present above 30 m. At 0.5 m, Ni was bound to colloidal DOM (6%) and oxyhydroxides (33%). Below 10 m the colloidal Ni contribution was <1%, which might suggest that DOM-sized colloids are more important for Ni transport (as in D-pit); however, those particles are respired in deeper layers of the oxygenated DJX-pit. Arsenic concentrations were <1.5 ppb and colloidal As was only detected in the surface water sample (0.5 m), dominantly in the form of oxyhydroxides (9%).

Other metals that were largely represented in the oxyhydroxide fraction were Fe in the mixolimnia of the D-pit (32%) and DJX-pit (25%), and Co in the mixolimnion of the DJX-pit (24%). Despite the high concentrations of Mn in both pit lakes, only the D-pit showed the presence of colloidal Mn (up to 6%). Therefore, the observed oxyhydroxides are expected to contain mainly Al, and some Fe (mostly D-pit). The presence of such colloids was also predicted by PHREEQC calculations, which indicated

oversaturation for mineral phases, including boehmite, diaspore, nontronite, and hematite (Appendix 1, SI).

4.5 Microbial communities

The relative distribution of phylogenetic classes, as determined by 16S rRNA gene sequencing, revealed a high microbial diversity within the two pit lakes (Figure S8). Qualitatively, the classes with the highest representation in the water column were Alphaproteobacteria, Betaproteobacteria, Gammaproteobacteria, Actinobacteria, and Flavobacteria. Metal reduction studies in groundwater have suggested that Actinobacteria are most active at circumneutral pH and when NO_3^- is absent (Williams *et al.*, 2013), which was the case for the two pit lakes. In the D-pit, the classes Acidobacteria, Holophagae, and Acidimicrobia were found in greater abundance than in the DJX-pit, whereas the latter showed a higher abundance of Sphingobacteria. The calculated Shannon diversity indices were highest close to the chemoclines in both pits (Figure S9). Specifically, the highest indices were found for D-pit at 5 m depth (7.1), followed by DJX-pit at 70 m (6.9) and D-pit at 15 m (6.4). Lowest diversity indices were calculated for DJX-pit at 20 m (5.0) and D-pit at 0 m (4.6). The highest microbial diversity in the D-pit was, therefore, linked to the thermocline around 5 m and the redox transition zone with the highest ORP gradient at 15 m. Similarly, in DJX-pit, the diversity increase was related to the deep chemocline at 65 m. These findings are consistent with other authors (Falagán *et al.*, 2013, 2014) that showed that highest diversity and abundance in meromictic lakes is linked to the chemoclines.

The dominant prokaryotic taxa are summarized in Table S13 (SI). One of the most abundant species in both pits was a close relative to *Arthrobacter sp.*, an Mn(II)-oxidizing species which has been previously identified at uranium mine sites (Bohu *et al.*, 2016). Its highest abundance was observed at 20 m depth of the DJX-pit, where an increase in Mn concentrations from 0.1 ppm to over 2 ppm occurred. A close relative to another dominant species, *Alkaliphilus peptidifermentans strain Z-7036*,

was particularly abundant at the depth of the thermocline. This spore-forming aerotolerant anaerobic organism is known to reduce Fe(III) (Zhilina *et al.*, 2009). Microorganisms closely related to those associated with U(VI) reduction, such as *Desulfosporosinus orientis* (also SO_4^{2-} reducing), *Clostridium acetobutylicum, Geobacter uraniireducens*, *Geobacter metallireducens*, and *Geobacter sulfurreducens* (Williams *et al.*, 2013), were also found in both pit lakes. Species of the named genera were previously shown to be stimulated during in situ U(VI) reduction experiments (e.g., Xu *et al.*, 2010; Van Nostrand *et al.*, 2011; Alessi *et al.*, 2014). With the exception of the close relative to *Geobacter sulfurreducens*, the species discussed above were more abundant in D-pit than DJX-pit, especially close to the chemocline (10 m sample). *Geobacter uraniireducens* is mainly an Fe(III)-and Mn(IV)-reducing microorganism, which can grow at temperatures above 10°C (Shelobolina *et al.*, 2008). Its growth might be seasonally limited to the water layers above the thermoclines of the pits at 5 m (D-pit) and 20 m (DJX-pit), respectively. The pH range below 5 m depth may further limit growth, as *Geobacter uraniireducens* is best suited to pH conditions between 6.0-7.7. Despite those limitations, a microorganism most closely related to *Geobacter uraniireducens* was present in all water depths of both pit lakes. A bacterium related to *Geobacter metallireducens*, a strict anaerobic bacterium capable of reducing Fe(III), Mn(IV), and U(IV) (Lovley *et al.*, 1993), was detected in deeper layers of the DJX-pit (70 m) and D-pit (15 m). Also capable of U(VI) reduction, *Desulfosporosinus orientis DSM 765* is a strictly anaerobic Gram-negative bacterium, which can grow chemoheterotrophically using SO_4^{2-} or thiosulfate as electron acceptors, or autotrophically with hydrogen and SO_4^{2-} (Stackebrandth *et al.*, 1997). A close relative to this bacterium was less abundant in the DJX-pit than the D-pit, even with the higher concentrations of U and SO_4^{2-}, highlighting its preference for anoxic environments.

One Betaproteobacterium species was most closely related to *Rhodoferax ferrireducens*. This phototrophic bacterium was more abundant in D-pit, especially at the chemocline, which was consistent with the concentrations of Fe(II) found in this pit. Another bacterium, which is often found

with higher Fe concentrations is *Sideroxydans lithotrophicus*, which is known to oxidize Fe(II) (Emerson and Moyer, 1997); a close relative was abundant in deeper layers of the D-pit where higher Fe concentrations prevailed. Bacteria possibly capable of As(III) oxidation were found in both pits, such as representatives of the genus *Rhizobium* (Campos *et al.*, 2009; see Appendix 2, SI) or some *Pseudomonas* strains (Paul *et al.*, 2014). A Betaproteobacterium most closely related to the As(III)-oxidizing bacterium *C05* was only found in the D-pit and predominantly in the mixolimnion. Representatives of the previously described genera *Geobacter*, *Desulfosporosinus,* and additionally *Alkaliphilus,* are all capable of dissimilatory As(V) reduction (Giloteaux *et al.*, 2013). Microorganisms from these genera were found in both pits, but they were more abundant in the zone close to the chemocline of the D-pit.

5 Discussion

5.1 Geochemical metal cycling

In both pit lakes, meromixis influences the cycling of the major contaminants, especially U and As. Both pit lakes had pH >7 at the surface and were likely influenced by photosynthesis and CO_2 exchange with the atmosphere that can lead to strong carbonate complexation of U. Due to intrinsic acid generation from the surrounding waste rocks and aerobic respiration of organic materials, the pH dropped with increasing depth (Figure 3). However, the sharp change in the ORP in the D-pit prevented the acidification below the chemocline as a consequence of Fe(III) and SO_4^{2-} reduction, metabolisms that both lead to the generation of bicarbonate (Boehrer and Schultze, 2008; Geller *et al.*, 2012). Iron in general was one of the drivers for the stratification of the D-pit (Boehrer and Schultze, 2008; Bohrer *et al.*, 2017). Additionally, this Fe cycling could be the key driver for U concentration changes in this pit, as summarized in Figure 6. The Fe and U redox couples have similar potentials and small changes in water chemistry can turn reducing agents into oxidizing agents (Du *et al.*, 2011). For instance, Fe(II) could diffuse upwards through the chemocline to reduce U(VI) (Liger *et al.*, 2009). This leads to U(IV) precipitates forming above the chemocline, which could then drive down the total

U concentration just above the chemocline. U(IV) precipitates might subsequently get oxidized back to soluble U(VI) by forming Fe(III)-bearing colloids, causing an increase in total U at 13 m depth; this is supported by oxygenic photosynthesis at this depth (Figure S11). Below the chemocline, alkaline conditions lead to strong carbonate complexation of U(VI), which was supported by the increasing TIC concentrations (Figure 4). Carbonate complexation prevents U(VI) from being reduced completely by Fe(II) and S(-II) (Anderson *et al.*, 1989). The reductive dissolution of amorphous Fe(III) oxyhydroxides, and other Fe minerals in the D-pit, release mineral-bound and co-precipitated As causing its concentrations to rise below 13 m depth. Reducing conditions also favored the formation of organic colloids that can contribute to the Ni and As transport (Figure 5).

Colloids in the D-pit might also contribute to U cycling by scavenging U(VI) from the water column. Indeed, speciation models for the mixolimnion predicted a decrease in negatively charged U(VI) species due the decreasing pH (Table 3). The anionic species, $UO_2(CO_3)_2^{2-}$ and $UO_2(CO_3)_3^{4-}$, are calculated to make up approximately 86% of all U species at 0.5 m. This fraction decreased to 35% at 5 m and 24% at 10 m, concomitant with the neutrally charged $UO_2CO_3^0$ becoming the dominant species. At a pH of 6.0-6.5, $UO_2CO_3^0$ is more likely to sorb to hydroxyl groups of the oxyhydroxide colloids, which can agglomerate to form larger particles and remove U from solution. At the chemocline, aqueous U(IV) was predicted to be present mostly as $U(OH)_5^-$. However, the abundance of Fe or Al oxyhydroxide colloids progressively decreased with depth, and in the monimonlimnion, DOM became the dominant U bearing colloidal phase (up to 8% of total U). In the D-pit, the oxyhydoxides also played an important role for As, and hosted up to 42% of the total As in the mixolimnion (Figure 5), which was likely due to As co-precipitation onto Fe oxyhydroxide particles (Slowey *et al.*, 2007).

Meromixis in the DJX-pit was predicted by Dessouki *et al.* (2005), who performed phosphate fertilization experiments in the pit before it was completely flooded. In the DJX-pit no change in ORP

was observed and the pH dropped to 5.5 after the first chemocline (Figure 3). This pit illustrates a "stairs-like" meromixis type that could be influenced by Ca (Boehrer and Schultze, 2008; Boehrer *et al.*, 2017). The formation and precipitation of $CaCO_3$ in the upper 20 m, and its subsequent dissolution below the chemocline, might lead to the accumulation of Ca in deeper water layers, which further stabilized the stratification (Figure 6). The DJX-pit might also be influenced by Mn cycling (Boehrer and Schultze, 2008; Boehrer *et al.*, 2017). Mn(IV)-oxides could be precipitating in the well oxygenated water but then get reduced to Mn(II) at the very bottom of the water column, inducing a rise of Mn concentrations which would increase stratification stability. A similar "stairs-like" meromixis was found in the Cueva de la Mora pit lake in Spain, which was not only due to double-diffusive convection processes but was likely also induced by sulfate- and metal-laden groundwater inputs entering the mine through intersecting galleries (Schultze *et al.*, 2017). Al-bearing colloids could be responsible for additional U accumulation in deeper water layers (Figure 5). Similarly, removal of As by precipitating Al oxyhydroxides was proposed by Sánchez-España *et al.* (2016) in the San Telmo acidic pit lake (Spain).

In general, due to the oxic conditions, colloidal transport of metals in the DJX-pit was limited to oxyhydroxide particles. There are a number of potential hypotheses that may explain the presence of oxygen in the lower layers of DJX-pit. For example, oxygen may still be present from the days of flooding, due to the low oxygen demand of deeper DJX-pit layers, or there may be oxygenated groundwater inputs to the lower layers (Geller *et al.*, 2012). Some of the wells located north of the DJX-pit, lying in an area that is hydrologically upgradient of the pit, were tested in June 2017 and found to contain oxygen. Examples are wells shown in Figure S1: HYD07-11G (11.8 m deep) with 3.1 mg/L oxygen and HYD06-03G (5.0 m deep) with 3.5 mg/L oxygen. Additionally, the bedrock in the mining area is fractured and weathered (AREVA, 2009), which may favor input of oxygenated groundwater. Therefore, the DJX-pit may not truly be meromictic, since, under this scenario, renewal

of the monimolimnion with oxygen-containing water is quite uncommon. Although groundwater inputs might destabilize the pit's stratification by reducing the salinity in the monimolimnion (Pieters and Lawrence, 2014), the opposite appears to be the case in the DJX-pit. The concentrations of SO_4^{2-}, Cl^-, B, Na, Ca, and Br found in the groundwater well GW2 (Tables S6 and S8), north of the DJX-pit, suggests that higher salinity groundwater is moving from the north towards the DJX-pit. This plume might be partially responsible for the chemocline at 65 m depth, bringing in not only the above mentioned anions and cations, but also Ni and U that had eluted from the waste rock in the backfilled DJN-pit and the adjoining bedrock (Figure 2). The observation of oxygen in the DJX-pit might be explained by occasional mixing processes. The shallower portion of the pit, over the backfilled DJN, could be cooling faster in the winter causing this oxygenated water to slide down toward deeper layers and leading to episodic deep water renewal, a process previously observed in Lake Malawi (Boehrer and Schultze, 2008). However, further investigations of the shallower portions of the pit would be needed to refine the understanding this and other potential sources of oxygen in the lower layers of the DJX-pit.

The high relative depth of both pit lakes is likely a key contributor to their stable stratification (Pieters and Lawrence, 2014). D-pit and DJX-pit have relative depths of 20% and 27%, respectively and formation of an ice cover every year promotes stable chemoclines in both pits. Factors that might disturb meromixis in the case of D-pit and DJX-pit are rock falls, landslides (Figure S10), surface water inputs, and potential changes in groundwater flow.

5.2 Microbial communities in comparison to acidic pit lakes

The overall microbial composition in the Cluff Lake pits was different from previously studied acidic (pH 2.5-4.5) pit lakes, such as Cueva de la Mora and Guadiana in Spain (Falagán *et al.*, 2013, 2014). Bacteria dominant in those two lakes, including *Leptospirillum sp.*, *Acidithiobacillus sp.*, *Metallibacterium sp.*, *Thiomonas sp.*, and *Desulfomonile sp.*, were not detected in the Cluff Lake pits

(Appendix 2). Generally, compared to the acidic pit lakes, Acidobacteria and Deltaproteobacteria were less abundant in the Cluff Lake pits (Figure S8). On the other hand, bacteria reported to be related to *Desulfosporosinus sp.* (see above) were found, and they were more dominant in the pH-neutral D-pit, likely due to the anoxic conditions found there (Falagán *et al.*, 2014). Relatives of the acidophilic and aerobic bacterium *Alicyclobacillus sp.* (Chang and Kang, 2004), which was previously identified in acidic pit lakes (Falagán *et al.*, 2013, 2014) were also found at the chemocline of the D-pit. Falagán *et al.* (2014) identified various archaea of the order Thermoplasmatales and the phyla Thaumarchaeota and Crenarchaeota in the acidic pit lakes. In this study, relatives of Thermoplasmates were identified mostly in the DJX-pit and Thaumarchaeota were only detected in the water column of the D-pit (Appendix 2). Crenarchaeota were not detected in either of the pits.

5.3 Potential for enhanced remediation

The meromictic behavior of the investigated pit-lakes opens potential opportunities by enhancing the use of pit lakes as a remediation strategy by promoting metal precipitation in the monimolimnia (Fisher and Lawrence, 2006; Pieters and Lawrence 2014). For example, the application of fertilizer over longer time periods would enhance algal growth in the mixolimnion, which may lead to enhanced metal removal from this layer through metal sorption and uptake by algal cells, as demonstrated previously over a shorter term in the DJX-pit by Dessouki *et al.* (2005). Fertilization with phosphorus was observed to increase the removal of metals (e.g., U, Ni, Zn, Mn, Cu, As) from the surface water and their accumulation the sediments. Metal removal through fertilization was also achieved in the Island Copper Mine pit lake (Canada) through the addition of nitrogen and phosphorus (Schultze *et al.*, 2017). An additional effect of fertilization could be the stimulation of sulfate-reducing bacteria (such as *Desulfosporosinus orientis*) in the monimolimnion, which would promote the formation of insoluble sulfide minerals, such as NiS, in the DJX-pit. Arsenic sulfides might form and could lead to the coprecipitation of As(III) with ferrous sulfides in the D-pit, as been seen in the Cueva de la Mora pit (Schultze *et al.*, 2016). Similarly, in the Island Copper Mine pit lake, metal removal from the

mixolimnion through the formation of sulfides at the chemocline was found to be an efficient process (Schultze *et al.*, 2017).

The formation of insoluble sulfides might also lead to the development of a significant U sink, as sulfide particles can remove U from the water column though sorption (Wersin *et al.*, 1994; Diez-Ercilla *et al.*, 2014). Moreover, reducing conditions could promote the precipitation of U(IV) through *Desulfosporosinus orientis*, *Geobacter* species or other U(VI)-reducing organisms, when sufficient electron donors are available (Williams *et al.*, 2013). Differing remediation approaches would likely be required between D-pit and DJX-pit, as their redox conditions vary considerably. The presence of oxygen in deeper layers of the DJX-pit, if it persists, could influence remediation outcomes. The formation of anoxia in the DJX-pit through fertilization could initiate the formation of sulfides and U(IV) precipitation, but they are likely to already take place in the D-pit. In contrast, the addition of sulfate, e.g., as gypsum (Lueders and Friedrich, 2002; Kijjanapanich *et al.*, 2014), to D-pit might provide an electron acceptor for SO_4^{2-} reducing bacteria, including those which are known to actively reduce U(VI). Additionally, iron sulfides (e.g., mackinawite) might form and abiotically reduce U(VI) (Bargar *et al.*, 2013; Veeramani *et al.*, 2013; Alessi *et al.*, 2014). Although reducing conditions are known to increase the bioaccessibility of As, in the long term, precipitates such as orpiment (As_2S_3) and realgar (AsS) might partially remove As from the water column (Appendix 1, SI).

6 Conclusions

Our study provides new insights on the geochemical behavior of dissolved and colloidal metals in meromictic pit lakes in a subarctic climate. Meromixis was found to determine the metal distribution, speciation and colloidal formation in the pit lakes at Cluff Lake. The redox state and mineral composition of the bedrocks of the pits have led to the formation of two types of stratification. Strong reducing conditions in the monimolimnion of the D-pit led to increased As concentrations (mostly As(III) species), but did not promote the precipitation of reduced U minerals, likely due to U

554 stabilization by carbonate complexation. The chemocline of this pit is a highly dynamic zone,
555 governed by the cycling of Fe. In contrast, the oxic conditions and high Ca and Mg concentrations in
556 the DJX-pit with a staircase-like stratification, led to low As concentrations in the water column and an
557 accumulation of U and Ni at the pit bottom. In both pits the association of metals with colloidal
558 particles could be observed. Potential U(VI)-reducing microorganisms were mostly found near the
559 chemocline of the D-pit and in deeper layers of the DJX-pit, and some of those microorganisms are
560 known to reduce As(V). Further investigations at the Cluff Lake mine pits should focus on the
561 speciation and size distribution of contaminant bearing colloids, and the U, As, and Ni distribution and
562 speciation in the sediments of the pit lakes.

563 Acknowledgments

564 This work was supported by Natural Sciences and Engineering Research Council of Canada (NSERC)
565 Discovery grants to D.S.A. (RGPIN-04134) and K.O.K. (RGPIN-165831), by a 2015-2016 Ashley and
566 Janet Cameron Research and Education Seed Fund grant to D.S.A., and by a 2016-2017 University of
567 Alberta Northern Research Award to T.W. The authors would like to thank to AREVA Resources
568 Canada and CanNorth for the provided data and samples, borrowed equipment, technical support, and
569 in-kind contributions. The authors further appreciate the support provided by Chad Cuss and
570 Alexandre Bagnoud, and would like to thank the two anonymous reviewers for their valuable
571 suggestions and comments.

572 Tables

573 Table 1: Fe(II) and total Fe concentration determined by the ferrozine absorption method in the D-
574 pit and the groundwater well close to it (GW1: DWW0041G. “n.d.”: not detected).

Depth (m)	Total Fe	Fe(II)	
	ppm	ppm	% (of total)
0.5	n.d.	n.d.	-
5	0.92 ± 0.31	0.09 ± 0.13	9.7
10	1.26 ± 0.54	0.28 ± 0.22	22.7
15	52.25 ± 2.21	41.83 ± 1.02	80.1
20	51.59 ± 2.69	40.02 ± 1.60	77.6
GW1	0.93 ± 0.06	0.29 ± 0.03	31.4

Table 2: IC-ICP-MS results for As speciation in the D-pit and total As based on iCAP Q ICP-MS.

Depth (m)	Total As	As(V)		As(III)	
	ppb	ppb	% (of total)	ppb	% (of total)
0.5	1.58	0.94	59.5	0.54	34.2
5	2.45	1.12	45.7	0.63	25.7
10	3.56	1.68	47.2	0.95	26.7
13	16.52	2.91	17.6	14.41	87.2
15	46.83	8.72	18.6	41.47	88.6
18	75.38	12.91	17.1	70.38	93.4
20	69.87	12.05	17.2	61.38	87.8
23	85.43	12.15	14.2	77.05	90.2

Table 3: PHREEQC modeling results for U, As, and Ni at selected depths. The distribution of major calculated species (in %) and the saturation indices (Sat Ind) for solid species are shown. A similar table with molar concentrations can be found in the SI (Table S11). The full output can be found in Appendix 1 (SI).

			D-pit					DJX-pit		
Element	Ox. state	Species	0.5 m	5 m	10 m	13 m	20 m	0.5 m	50 m	80 m
U	U(IV)	$U(OH)_5^-$	0%	0%	0%	98%	100%	0%	0%	0%
		$U(OH)_4$	0%	0%	0%	1%	0%	0%	0%	0%
	U(VI)	$UO_2(CO_3)_2^{2-}$	83%	34%	24%	0%	0%	71%	1%	0%
		UO_2CO_3	14%	65%	75%	0%	0%	26%	77%	56%
		$UO_2(CO_3)_3^{4-}$	3%	1%	0%	0%	0%	2%	0%	0%
		UO_2OH^+	0%	0%	0%	0%	0%	1%	6%	9%
		UO_2^{2+}	0%	0%	0%	0%	0%	0%	10%	17%
		UO_2SO_4	0%	0%	0%	0%	0%	0%	4%	11%
	Sat Ind	U_3O_8	-3.7	-4.6	-4.3	-3.0	-16.0	-1.3	-2.8	0.6
		U_4O_9	-6.4	-4.1	-3.1	14.3	4.3	-2.4	-3.7	1.7
		UO_2	-2.7	-1.7	-1.3	5.4	4.0	-1.6	-1.9	-0.4
		$USiO_4$	-3.7	-2.4	-2.0	4.8	3.3	-2.8	-2.5	-1.0
As	As(III)	H_3AsO_3	0%	0%	1%	100%	98%	0%	0%	0%
		$H_2AsO_3^-$	0%	0%	0%	0%	2%	0%	0%	0%
	As(V)	$HAsO_4^{2-}$	77%	32%	25%	0%	0%	77%	8%	10%
		$H_2AsO_4^-$	23%	68%	75%	0%	0%	23%	92%	90%
Ni		$NiCO_3$	79%	31%	22%	50%	96%	52%	0%	0%
		Ni^{2+}	19%	63%	72%	45%	4%	40%	80%	72%
		$NiHCO_3^+$	2%	5%	5%	5%	1%	2%	0%	0%
		$NiSO_4$	0%	0%	1%	0%	0%	6%	19%	28%

Figure captions

Figure 1: (Left) The Athabasca Basin (light shape), the Carswell Structure (dark round shape), and the location of the former Cluff Lake uranium mine (mining symbol). (Right) The mining area with the meromictic pit lakes (D-pit and DJN/DJX-pits). For a more detailed map and corresponding geochemical data see Figure S1 and Table S1 (SI). GIS data provided by AREVA.

Figure 2: Schematic cross section through the DJX-pit (information provided by AREVA) and D-pit (rough estimation) showing the 3 different water layers in each pit. For comparison, the relative vertical positions and dimensions of the groundwater wells GW1 and GW2 are shown. The orientation of the cross sections is shown at the bottom. Vertical exaggeration is 6.5x. The curved blue arrows indicate potential groundwater inflow pathways. See Figure S12 for a 3D DJX-pit model and for spatial location of GW2.

Figure 3: Limnological results (temperature, pH, specific conductivity, dissolved oxygen, and oxidative-reductive potential (ORP)) for D-pit (left) and DJX-pit (right) measured at the Cluff Lake site. Note the differences in depth (vertical scale) between the two pits.

Figure 4: Measured cations, anions, carbon and nitrogen in the D-pit (left) and the DJX-pit (right) in June 2016.

Figure 5: Colloidal distribution of dissolved, organic matter associated (DOM), and oxyhydroxide associated (Oxyhyd) U, Ni, and As in the D- and DJX-pit lakes. Distribution of other metals can be found in Tables S9-S10. Example fractograms for U, Ni, and As are presented in Figure S7 (SI).

Figure 6: Schematic summary of ongoing processes influencing the stratification and distribution of U in both pits. In the D-pit (left) the Fe cycling drives the reduction and oxidation of U in the mixolimnion and at the chemocline, together with photosynthesis. Carbonate complexation in deeper water layers keep U(VI) in solution even under anoxic solutions. In the DJX-pit (right) Ca cycling is the driving force behind the stratification and Al oxyhydroxides drive the accumulation of U in deeper water layers.

References

Alessi, D.S., Lezama-Pacheco, J.S., Janot, N., Suvorova, E.I., Cerrato, J.M., Giammar, D.E., Davis, J.A., Fox, P.M., Williams, K.H., Long, P.E., Handley, K.M., Bernier-Latmani, R., Bargar, J.R. 2014. Speciation and reactivity of uranium products formed during in situ bioremediation in a shallow alluvial aquifer. Environmental Science & Technology, 48(21): 12842-12850.

Anderson, R. F., Fleisher, M. Q., and LeHuray, A. P. 1989. Concentration, oxidation state, and particulate flux of uranium in the Black Sea. Geochimica et Cosmochimica Acta, 53(9): 2215-2224.

AREVA. 2009. Cluff Lake project. Detailed decommissioning plan, version 2. AREVA Resources Canada Inc.

AREVA. 2013. Cluff lake project: 2012 annual report. AREVA Resources Canada Inc.

Bargar, J.R., Williams, K.H., Campbell, K.M., Long, P.E., Stubbs, J.E., Suvorova, E.I., Lezama-Pacheco, J.S., Alessi, D.S., Stylo, M., Webb, S.M., Davis, J.A., Giammar, D.E., Blue, L.Y., and Bernier-Latmani, R. 2013. Uranium redox transition pathways in acetate-amended sediments. Proceedings of the National Academy of Sciences, 110(12): 4506-4511.

Bell, K. 1985. Geochronology of the Carswell area, northern Saskatchewan. In: The Carswell Structure Uranium Deposits, Saskatchewan. Geological Association of Canada Special Paper, 29: 34-46.

Boehrer B., von Rohden C., Schultze M. 2017. Physical Features of Meromictic Lakes: Stratification and Circulation. In: Gulati R., Zadereev E., Degermendzhi A. (eds) Ecology of Meromictic Lakes. Ecological Studies (Analysis and Synthesis), vol 228. Springer, Cham

Boehrer, B., and Schultze, M. 2008. Stratification of lakes. Reviews of Geophysics, 46(2).

Bohu, T., Akob, D. M., Abratis, M., Lazar, C. S., and Küsel, K. 2016. Biological low-ph mn(ii) oxidation in a manganese deposit influenced by metal-rich groundwater. Applied and Environmental Microbiology, 82(10): 3009-3021.

Campos, V. L., Escalante, G., Yañez, J., Zaror, C. A., and Mondaca, M. A. 2009. Isolation of arsenite-oxidizing bacteria from a natural biofilm associated to volcanic rocks of Atacama Desert, Chile. Journal of Basic Microbiology, 49(S1).

Chang, S. S., and Kang, D. H. 2004. Alicyclobacillus spp. in the fruit juice industry: history, characteristics, and current isolation/detection procedures. Critical Reviews in Microbiology, 30(2): 55-74.

Church, C.D., Wilkin, R.T., Alpers, C.N., Rye, R.O., and McCleskey, R.B. 2007. Microbial sulfate reduction and metal attenuation in pH 4 acid mine water. Geochemical Transactions, 8(1): 10.

Cuss, C.W., and Guéguen, C. 2012. Determination of relative molecular weights of fluorescent components in dissolved organic matter using asymmetrical flow field-flow fractionation and parallel factor analysis. Analytica Chimica Acta, 733: 98-102.

Dai, M., Martin, J.M., and Cauwet, G. 1995. The significant role of colloids in the transport and transformation of organic carbon and associated trace metals (cd, cu and ni) in the Rhône delta (France). Marine Chemistry, 51(2): 159-175.

Dessouki, T.C., Hudson, J.J., Neal, B.R., and Bogard, M.J. 2005. The effects of phosphorus additions on the sedimentation of contaminants in a uranium mine pit-lake. Water Research, 39(13): 3055-3061.

Diez-Ercilla, M., Sánchez-España, J., Yusta, I., Wendt-Potthoff, K., and Koschorreck, M. 2014. Formation of biogenic sulphides in the water column of an acidic pit lake: biogeochemical controls and effects on trace metal dynamics. Biogeochemistry, 121(3): 519-536.

Donahue, R., Hendry, M.J., and Landine, P. 2000. Distribution of arsenic and nickel in uranium mill tailings, Rabbit Lake, Saskatchewan, Canada. Applied Geochemistry, 15(8): 1097-1119.

Donner, M.W., Javed, M.B., Shotyk, W., Francesconi, K.A., and Siddique, T. 2017. Arsenic speciation in the lower Athabasca River watershed: a geochemical investigation of the dissolved and particulate phases. Environmental Pollution, 224: 265-274.

Du, X., Boonchayaanant, B., Wu, W.M., Fendorf, S., Bargar, J., and Criddle, C.S. 2011. Reduction of uranium (VI) by soluble iron (II) conforms with thermodynamic predictions. Environmental Science & Technology, 45(11): 4718-4725.

Emerson, D., and Moyer, C. 1997. Isolation and characterization of novel iron-oxidizing bacteria that grow at circumneutral ph. Applied and Environmental Microbiology, 63(12): 4784-4792.

Falagán, C., Sánchez-España, F. J., and Johnson, D. B. 2013. Microbiological communities in two acidic mine pit lakes in the Iberian Pyrite Belt (IPB), Spain. Advanced Materials Research , 825: 19-22.

Falagán, C., Sánchez-España, J., and Johnson, D. B. 2014. New insights into the biogeochemistry of extremely acidic environments revealed by a combined cultivation-based and culture-independent study of two stratified pit lakes. FEMS microbiology ecology, 87(1): 231-243.

Filella, M. 2006. Colloidal Properties of Submicron Particles in Natural Waters. In: Environmental Colloids and Particles: Behaviour, Separation and Characterisation, Volume 10 (eds K. J. Wilkinson and J. R. Lead), John Wiley & Sons, Ltd, Chichester, UK.

Fisher, T.S., and Lawrence, G.A. 2006. Treatment of acid rock drainage in a meromictic mine pit lake. Journal of Environmental Engineering, 132(4): 515-526.

Geller, W., Schultze, M., Kleinmann, B., and Wolkersdorfer, C. 2012. Acidic pit lakes: the legacy of coal and metal surface mines. Springer Science & Business Media.

Giloteaux, L., Holmes, D.E., Williams, K.H., Wrighton, K.C., Wilkins, M.J., Montgomery, A.P., Smith, J.A., Orellana, R., Thompson, C.A., Roper, T.J., and Long, P.E. 2013. Characterization and transcription of arsenic respiration and resistance genes during in situ uranium bioremediation. The ISME Journal, 7(2): 370-383.

Guéguen, C., and Cuss, C.W. 2011. Characterization of aquatic dissolved organic matter by asymmetrical flow field-flow fractionation coupled to uv-visible diode array and excitation-emission matrix fluorescence. Journal of Chromatography A, 1218(27): 4188-4198.

Harper C.T. 1981. Geology of the Carswell Structure, central part. Saskatchewan Geological Survey Report 214. Available from publications.gov.sk.ca/documents/310/90719-Report-214_Geology_Of_The_Carswell_Structure-Central_Part.pdf [cited December 2016]

Jaeger, D. 1994. Effects of hypolimnetic water aeration and iron-phosphate precipitation on the trophic level of Lake Krupunder. Hydrobiologia, 275(1): 433-444.

Kijjanapanich, P., Annachhatre, A.P., Esposito, G., and Lens, P.N. 2014. Use of organic substrates as electron donors for biological sulfate reduction in gypsiferous mine soils from Nakhon Si Thammarat (Thailand). Chemosphere, 101: 1-7.

Kyser, K., and Michel, C. 2008. Unconformity-related uranium deposits. Mineralogical Association of Canada. Short Course Series, 39: Quebec, Mineralogical Association of Canada, 7-95.

Leigh, M.B., Wu, W.M., Cardenas, E., Uhlik, O., Carroll, S., Gentry, T., Marsh, T.L., Zhou, J., Jardine, P., Criddle, C.S., and Tiedje, J.M. 2015. Microbial communities biostimulated by ethanol during uranium (vi) bioremediation in contaminated sediment as shown by stable isotope probing. Frontiers of Environmental Science & Engineering, 9(3): 453-464.

Liger, E., Charlet, L., and van Cappellen, P. 1999. Surface catalysis of uranium (VI) reduction by iron (II). Geochimica et Cosmochimica Acta, 63(19): 2939-2955.

Lovley, D. R., Giovannoni, S. J., White, D. C., Champine, J. E., Phillips, E. J. P., Gorby, Y. A., and Goodwin, S. 1993. Geobacter metallireducens gen. nov. sp. nov., a microorganism capable of coupling the complete oxidation of organic compounds to the reduction of iron and other metals. Archives of Microbiology, 159(4): 336-344.

Lueders, T., and Friedrich, M.W. 2002. Effects of amendment with ferrihydrite and gypsum on the structure and activity of methanogenic populations in rice field soil. Applied and Environmental Microbiology, 68(5): 2484-2494.

Neubauer, E., Kammer, F., and Hofmann, T. 2013. Using flowfff and hpsec to determine trace metal-colloid associations in wetland runoff. Water Research, 47(8): 2757-2769.

Paul, D., Poddar, S. and Sar, P. 2014. Characterization of arsenite-oxidizing bacteria isolated from arsenic-contaminated groundwater of west Bengal. Journal of Environmental Science and Health, Part A, 49(13): 1481-1492.

Pieters, R., and Lawrence, G.A. 2014. Physical processes and meromixis in pit lakes subject to ice cover. Canadian Journal of Civil Engineering, 41(6): 569-578.

Porsch, K., and Kappler, A. 2011. Feii oxidation by molecular o2 during hcl extraction. Environmental Chemistry, 8(2): 190-197.

Rhulmann, F. 1985. Mineralogy and metallogeny of uraniferous occurrences in the Carswell structure: in the Carswell structure uranium deposits, Saskatchewan. Geological Association of Canada Special Paper 29: 105-120.

Sánchez-España, J., Yusta, I., Gray, J., and Burgos, W.D. 2016. Geochemistry of dissolved aluminum at low pH: Extent and significance of Al–Fe (III) coprecipitation below pH 4.0. Geochimica et Cosmochimica Acta, 175: 128-149.

Schultze M., Boehrer B., Wendt-Potthoff K., Sánchez-España J., Castendyk D. 2017. Meromictic Pit Lakes: Case Studies from Spain, Germany and Canada and General Aspects of Management and Modelling. In: Gulati R., Zadereev E., Degermendzhi A. (eds) Ecology of Meromictic Lakes. Ecological Studies (Analysis and Synthesis), vol 228. Springer, Cham

Schultze, M., Castendyk, D., Wendt-Potthoff, K., Sánchez-España, J., and Boehrer, B. 2016. On the relevance of meromixis in mine pit lakes - an update. In: Proceedings IMWA 2016 Annual Conference, Freiberg, Germany. Available from www.imwa.info/docs/imwa_2016/IMWA2016_Schultze_27.pdf [cited December 2016]

Schüring, J., Schulz, H.D., Fischer, W.R., Böttcher, J., and Duijnisveld, W.H. 2013. Redox: fundamentals, processes and applications. Springer Science & Business Media.

Shelobolina, E.S., Vrionis, H.A., Findlay, R.H. and Lovley, D.R. 2008. Geobacter uraniireducens sp. nov., isolated from subsurface sediment undergoing uranium bioremediation. International Journal of Systematic and Evolutionary Microbiology, 58(5): 1075-1078.

Slowey, A.J., Johnson, S.B., Newville, M., and Brown, G.E. 2007. Speciation and colloid transport of arsenic from mine tailings. Applied Geochemistry, 22(9): 1884-1898.

Sobolewski, A. 1999. A review of processes responsible for metal removal in wetlands treating contaminated mine drainage. International Journal of Phytoremediation, 1(1): 19-51.

Stackebrandt, E., Sproer, C., Rainey, F. A., Burghardt, J., Päuker, O., and Hippe, H. 1997. Phylogenetic analysis of the genus Desulfotomaculum: evidence for the misclassification of Desulfotomaculum guttoideum and description of Desulfotomaculum orientis as Desulfosporosinus orientis gen. nov., comb. nov. International Journal of Systematic and Evolutionary Microbiology, 47(4): 1134-1139.

Stookey, L.L. 1970. Ferrozine---a new spectrophotometric reagent for iron. Analytical Chemistry, 42(7): 779-781.

Troyer, L.D., Stone, J.J., and Borch, T. 2014. Effect of biogeochemical redox processes on the fate and transport of as and u at an abandoned uranium mine site: an x-ray absorption spectroscopy study. Environmental Chemistry, 11(1): 18-27.

Vail, J. 2013. Groundwater sampling. Operating procedure. U.S. Environmental Protection Agency Science and Ecosystem Support Division. Athens, Georgia. Available from www.epa.gov/sites/production/files/2015-06/documents/Groundwater-Sampling.pdf [cited June 2017]

Van Nostrand, J.D., Wu, L., Wu, W.M., Huang, Z., Gentry, T.J., Deng, Y., Carley, J., Carroll, S., He, Z., Gu, B., and Luo, J. 2011. Dynamics of microbial community composition and function during in situ bioremediation of a uranium-contaminated aquifer. Applied and Environmental Microbiology, 77(11): 3860-3869.

Veeramani, H., Scheinost, A.C., Monsegue, N., Qafoku, N.P., Kukkadapu, R., Newville, M., Lanzirotti, A., Pruden, A., Murayama, M., and Hochella Jr, M.F. 2013. Abiotic reductive immobilization of U (VI) by biogenic mackinawite. Environmental Science & Technology, 47(5): 2361-2369.

Viollier, E., Inglett, P. W., Hunter, K., Roychoudhury, A. N., and Van Cappellen, P. 2000. The ferrozine method revisited: fe (ii)/fe (iii) determination in natural waters. Applied Geochemistry, 15(6): 785-790.

Wang, Y., Frutschi, M., Suvorova, E., Phrommavanh, V., Descostes, M., Osman, A. A., Geipel, G., and Bernier-Latmani, R. 2013. Mobile uranium (iv)-bearing colloids in a mining-impacted wetland. Nature Communications, 4.

Watson, D.B., Wu, W.M., Mehlhorn, T., Tang, G., Earles, J., Lowe, K., Gihring, T.M., Zhang, G., Phillips, J., Boyanov, M.I., and Spalding, B.P. 2013. In situ bioremediation of uranium with emulsified vegetable oil as the electron donor. Environmental Science & Technology, 47(12): 6440-6448.

Wersin, P., Hochella, M.F., Persson, P., Redden, G., Leckie, J.O., and Harris, D.W. 1994. Interaction between aqueous uranium (vi) and sulfide minerals: spectroscopic evidence for sorption and reduction. Geochimica et Cosmochimica Acta, 58(13): 2829-2843.

Williams, K.H., Bargar, J.R., Lloyd, J.R., and Lovley, D.R. 2013. Bioremediation of uranium-contaminated groundwater: a systems approach to subsurface biogeochemistry. Current Opinion in Biotechnology, 24(3): 489-497.

Williams, K.H., Long, P.E., Davis, J.A., Wilkins, M.J., N'Guessan, A.L., Steefel, C.I., Yang, L., Newcomer, D., Spane, F.A., Kerkhof, L.J., and McGuinness, L. 2011. Acetate availability and its influence on sustainable bioremediation of uranium-contaminated groundwater. Geomicrobiology Journal, 28(5-6): 519-539.

776 Xu, M., Wu, W.M., Wu, L., He, Z., Van Nostrand, J.D., Deng, Y., Luo, J., Carley, J., Ginder-Vogel,
777 M., Gentry, T.J., and Gu, B. 2010. Responses of microbial community functional structures to pilot-
778 scale uranium in situ bioremediation. The ISME Journal, 4(8): 1060-1070.

779 Zhilina, T. N., Zavarzina, D. G., Kolganova, T. V., Lysenko, A. M., and Tourova, T. P. 2009.
780 Alkaliphilus peptidofermentans sp. nov., a new alkaliphilic bacterial soda lake isolate capable of
781 peptide fermentation and fe (iii) reduction. Microbiology, 78(4): 445-454.

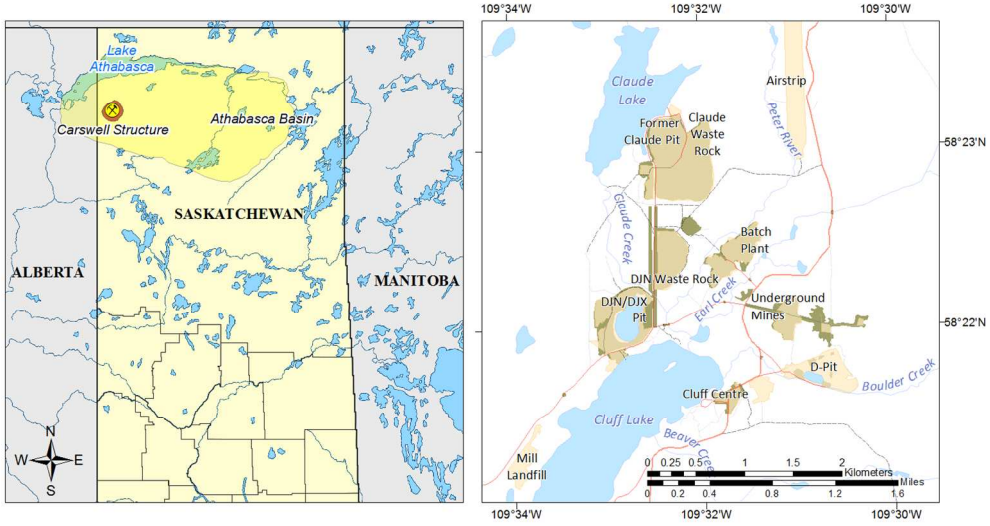

Figure 1: (Left) The Athabasca Basin (light shape), the Carswell Structure (dark round shape), and the location of the former Cluff Lake uranium mine (mining symbol). (Right) The mining area with the meromictic pit lakes (D-pit and DJN/DJX-pits). For a more detailed map and corresponding geochemical data see Figure S1 and Table S1 (SI). GIS data provided by AREVA.

411x215mm (96 x 96 DPI)

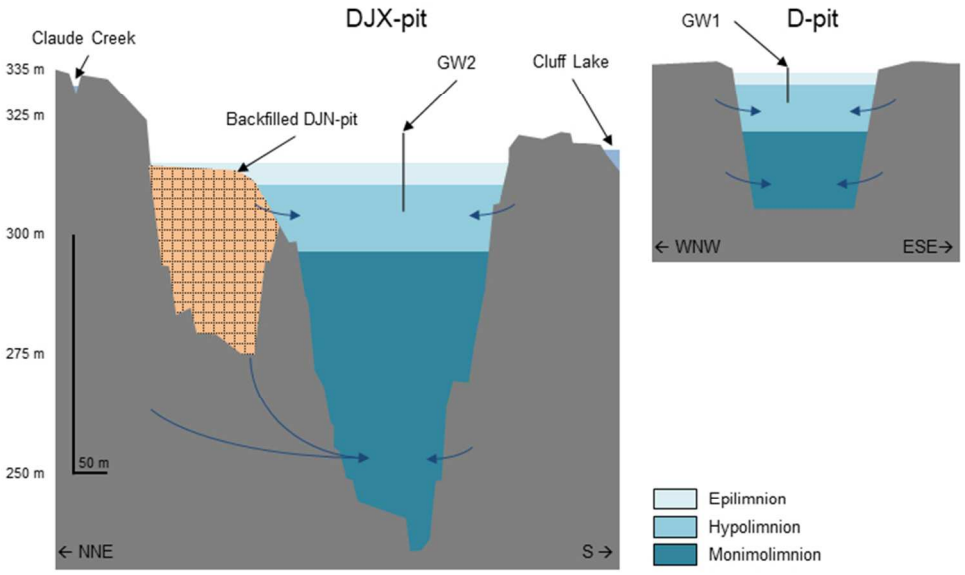

Figure 2: Schematic cross section through the DJX-pit (information provided by AREVA) and D-pit (rough estimation) showing the 3 different water layers in each pit. For comparison, the relative vertical positions and dimensions of the groundwater wells GW1 and GW2 are shown. The orientation of the cross sections is shown at the bottom. Vertical exaggeration is 6.5x. The curved blue arrows indicate potential groundwater inflow pathways. See Figure S12 for a 3D DJX-pit model and for spatial location of GW2.

204x124mm (96 x 96 DPI)

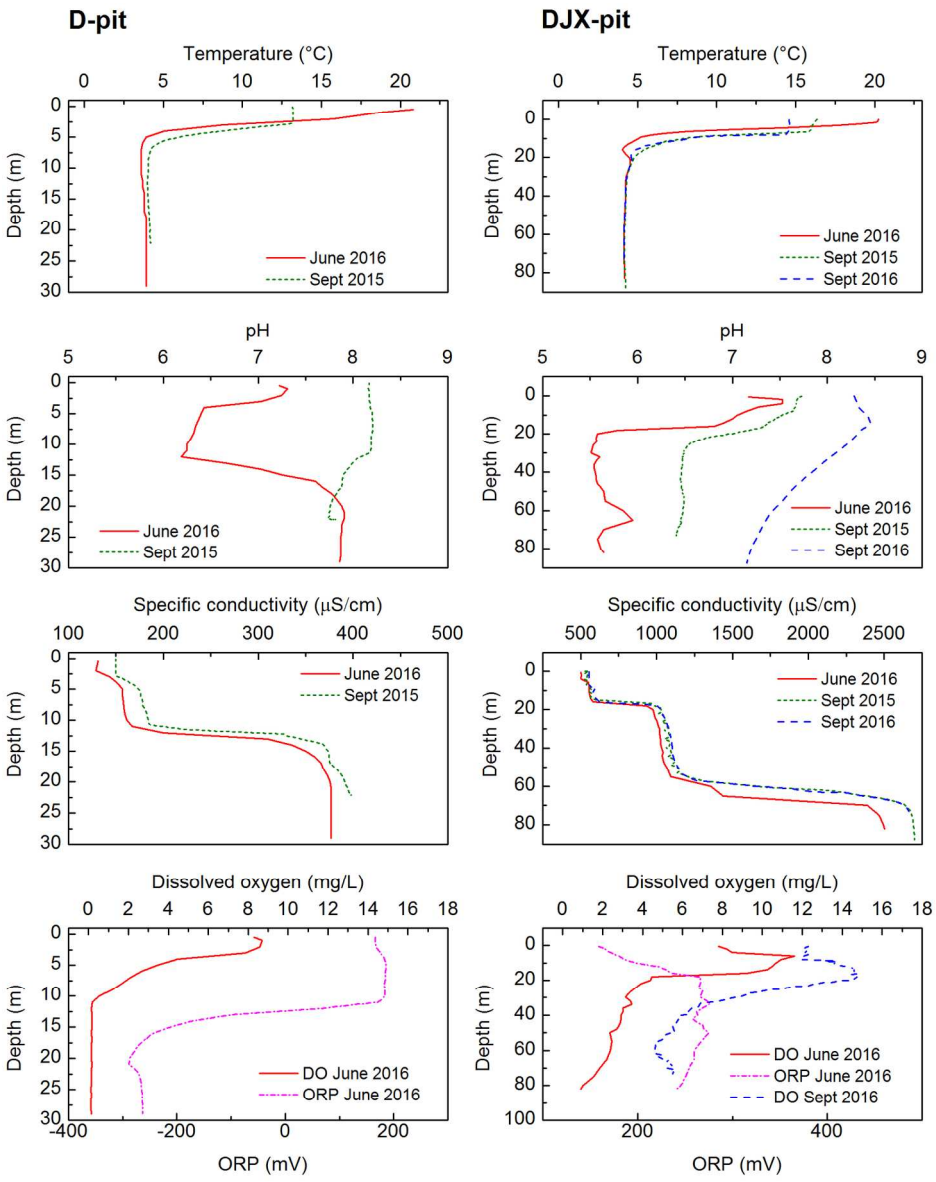

Figure 3: Limnological results (temperature, pH, specific conductivity, dissolved oxygen, and oxidative-reductive potential (ORP)) for D-pit (left) and DJX-pit (right) measured at the Cluff Lake site. Note the differences in depth (vertical scale) between the two pits.

170x215mm (300 x 300 DPI)

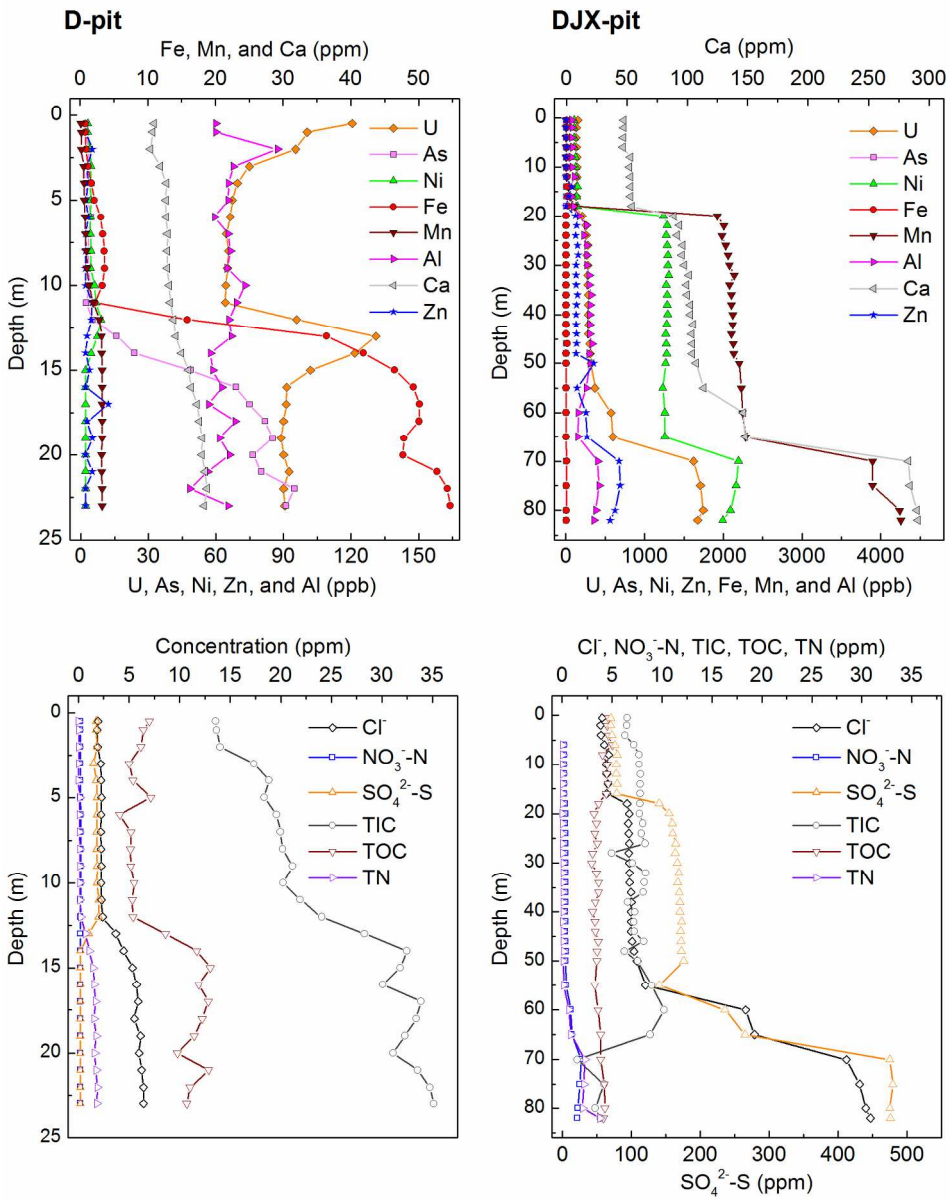

Figure 4: Measured cations, anions, carbon and nitrogen in the D-pit (left) and the DJX-pit (right) in June 2016.

169x215mm (300 x 300 DPI)

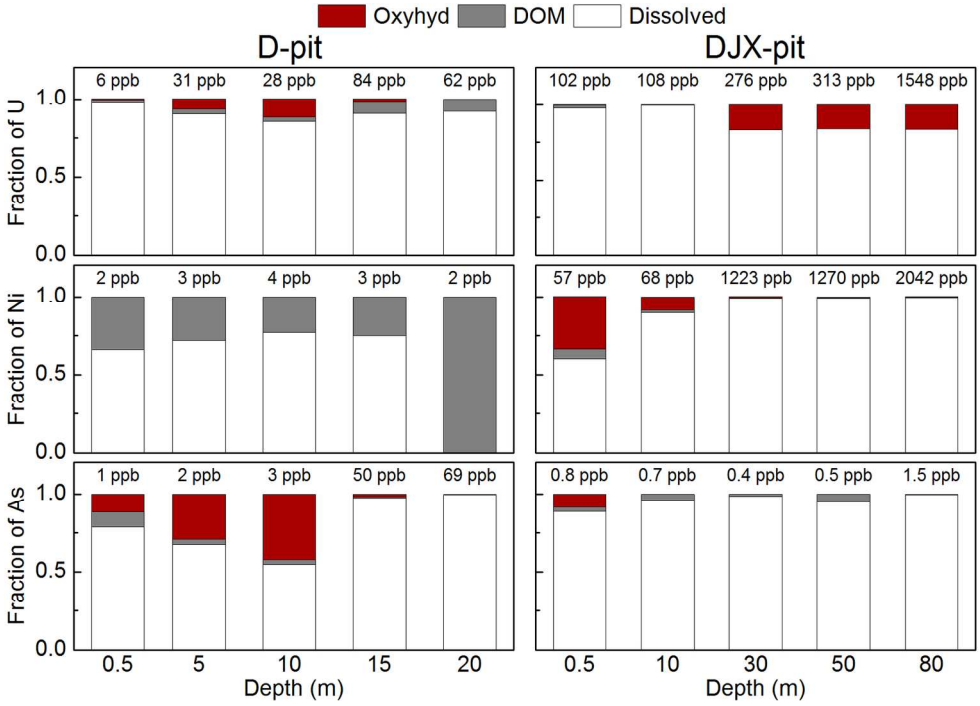

Figure 5: Colloidal distribution of dissolved, organic matter associated (DOM), and oxyhydroxide associated (Oxyhyd) U, Ni, and As in the D- and DJX-pit lakes. Distribution of other metals can be found in Tables S9-S10. Example fractograms for U, Ni, and As are presented in Figure S7 (SI).

170x118mm (300 x 300 DPI)

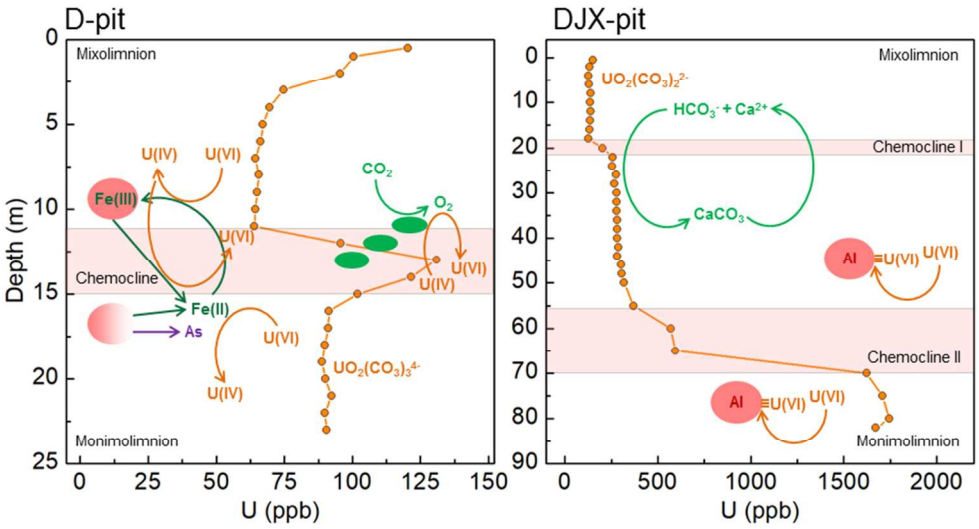

Figure 6: Schematic summary of ongoing processes influencing the stratification and distribution of U in both pits. In the D-pit (left) the Fe cycling drives the reduction and oxidation of U in the mixolimnion and at the chemocline, together with photosynthesis. Carbonate complexation in deeper water layers keep U(VI) in solution even under anoxic solutions. In the DJX-pit (right) Ca cycling is the driving force behind the stratification and Al oxyhydroxides drive the accumulation of U in deeper water layers.

250x134mm (96 x 96 DPI)